Rotaxane-Based Single Molecule Junctions for Memory Applications

Rotaxane-Based Single Molecule Junctions for Memory Applications

Roberto Listo*†, Fabrizio Mo*, Federico Ravera*, Andrea Vezzoli§,
Marco Vacca*, Gianluca Piccinini*, Mariagrazia Graziano‡ and Yuri Ardesi*¶
*Department of Electronics and Telecommunications, Politecnico di Torino, Torino 10129, Italy
†Department of Electrical, Computer and Biomedical Engineering, University of Pavia, Pavia 27100, Italy
‡Department of Applied Science and Technology, Politecnico di Torino, Torino 10129, Italy
§Department of Chemistry, University of Liverpool, Crown Street, Liverpool L69 7ZD, U.K.
¶Corresponding author e-mail: yuri.ardesi@polito.it

***Abstract*—As electronic components approach their fundamental physical limits, molecular electronics offer a promising alternative for next-generation computing and memory technologies. This simulative study explores the potential of rotaxane-based Single Molecule Junctions (SMJs) for memory applications. Through a combination of Molecular Dynamics (MD) simulations and Metadynamics (MetaD) analysis, we identify two distinct molecular states capable of encoding binary information. The energetic barriers to state transitions are evaluated, revealing the mechanisms for data encoding. Furthermore, electrical transport calculation demonstrates a significant current difference between the two configurations, supporting the feasibility of a current-driven readout for conformational-based memory. Our findings highlight the potential of rotaxane-based SMJs for non-volatile, high-density, low-power memory storage, positioning them as strong candidates for future molecular memories in nanocomputing applications.**

I. Introduction

Since the first demonstration of a working transistor at Bell Laboratories on December 23rd, 1947, continuous advancements in its design and scaling have driven the evolution of modern electronics. However, according to the 2023 International Roadmap for Devices and Systems (IRDS), this progress is approaching fundamental physical and economic limits, highlighting the need for alternative computing paradigms [1]. Among the Beyond-CMOS technologies, molecular electronics, particularly Single-Molecule Junctions (SMJs), have emerged as promising candidates, offering intrinsic miniaturization at the molecular scale, ultra-low power consumption, and high operational speed [2]–[4].

Fig. 1(a) depicts a SMJ consisting of two nanoelectrodes connected to a molecular unit via anchoring groups. Over the past five decades, the inherent tunability of SMJs enabled the development of a wide range of functionalities by properly designing the molecular structure. This versatility has led to the realization of molecular-scale components such as sensors, switches, diodes, and transistors, highlighting the potential of SMJs for future nanoscale electronic applications [4]–[6]. Furthermore, memory applications of single molecules devices have been proposed relying on different principles of operations, from position- to conformation-based memory cells [7]–[9].

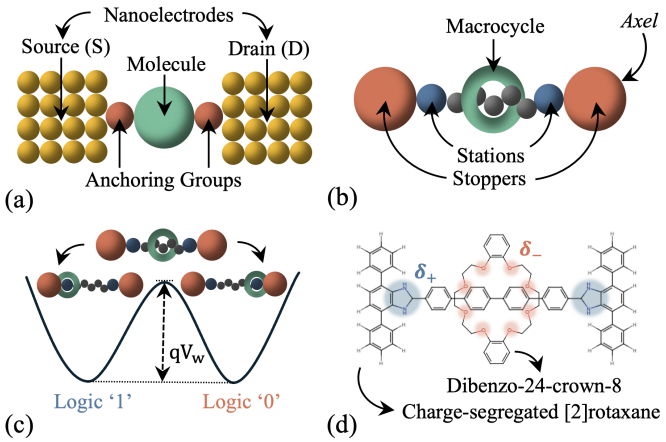

Fig. 1. (a) Sketch of an SMJ; (b) rotaxane molecule; (c) information encoding principle through the macrocycle position (qV_W is the separation energy barrier height); (d) structure formula of the considered rotaxane.

In 2016, Jean-Pierre Sauvage, Sir J. Fraser Stoddart, and Bernard L. Feringa were awarded the Nobel Prize in Chemistry for the design and synthesis of mechanically interlocked molecules, enabling controllable molecular motion [10]. Fig. 1(b) presents a schematic overview of a mechanically interlocked molecule, specifically a rotaxane. The rotaxane consists of a dumbbell-shaped molecular axle threaded through a ring called macrocycle. The macrocycle can be localized within specific regions in the axe, called stations. The axle is capped at both ends with bulky stoppers groups, preventing the ring from unthreading.

In this work, we assume that the binary information can be encoded in two distinct positions of the macrocycle along the molecular axis, as illustrated in Fig. 1(c). We thus investigate through *ab initio* and semi-empirical simulations an SMJ based on the rotaxane presented in [11], with the specific purpose of encoding binary information and performing electrical writing and reading of the memory state. Fig. 1(d) shows the structural formula of the rotaxane. We explore the stable rotaxane states and their energetic separation, enabling the non-volatile and re-writable information encoding. Our results demonstrate the potentiality of rotaxane-based molec-

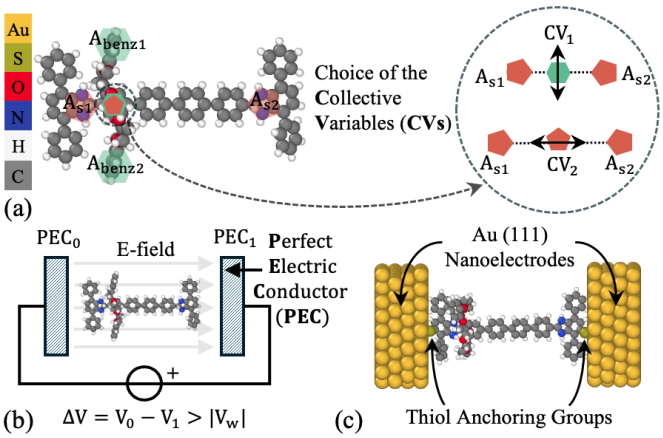

Fig. 2. (a) Scheme of the MetaD CVs choice; (b) Simulation setup for the MD simulation under PEC excitations; (c) Simulation scheme for the I(V) characterization of the SMJ.

ular junctions as electrically controllable memory elements, offering a pathway toward scalable, high-density, and low-power molecular data storage. By exploiting electric field-driven switching and current-based readout, this approach could enable a new class of molecular memories for future nanocomputing architectures, pushing the boundaries of miniaturization beyond conventional silicon technologies.

II. Theoretical Background and Computational Methods

A. Free Energy Profile

In rotaxane-based SMJs, the information encoding is controlled by electric fields generated by the two electrodes. We investigate the energy profile of macrocycle localization in the station through Metadynamics (MetaD) simulation to determine the applied voltage required for logical information encoding. The simulations are conducted trough QuantumATK v. 2024.09 and PLUMED [12]–[14]. Interatomic interactions were described by the `TorchX_MACE_MP_0_L2_2024` potential. The system is initialized with a Maxwell-Boltzmann velocity distribution at 300 K and coupled to a thermal reservoir maintained at the same temperature. To accurately describe the molecular motion, we select two collective variables (CVs) that characterize the shuttling process: the displacement of the geometrical center of the dibenzo-crown ether ring along the rotaxane axle (CV_1), and the intramolecular distance between the barycenter of the two benzene rings within the macrocycle (CV_2) as shown in Fig. 2(a). Such CVs enable comprehensive switching sampling, ensuring recrossing events between all metastable states and permitting for the reconstruction of the free energy profile. The combination of Langevin dynamics with metadynamics allowed for a controlled thermal environment while accelerating the sampling of rare events, facilitating a more comprehensive understanding of the molecular system's free-energy landscape. Moreover, a moving average filter was implemented to smooth random fluctuations, allowing for clearer visualization of transition states and underlying energy trends. The filtered data, F_{denoised}, is obtained as follows:

$$F(i) = F_{\text{denoised}}(i) = \frac{1}{N}\sum_{j=i}^{i+N} F_{sampled}(j) \tag{1}$$

where N represents the window size, set to 25 in this study. A larger N enhances noise suppression but may obscure fine details in the data, whereas a smaller N preserves details at the cost of reduced smoothing. The filtered dataset was subsequently used as input for Gaussian Process Regression (GPR) to generate the free energy profile.

B. Electric-Driven Simulations

We perform Molecular Dynamics (MD) simulations based on Machine-Learned Force Fields (ML-FF) using QuantumATK v. 2024.09. These simulations aim to derive two possible configurations in which the macrocycle can localize in the stations. The localization is induced by applying constant electric fields, which are enabled by the presence of Perfect Electric Conductors (PECs) [12]. Fig. 2(b) shows the simulation setup. By applying a voltage large enough to overcome the barrier threshold value found in the free energy profiling, we retrieve the two configurations corresponding to Logic '0' and '1'. The MD simulations are conducted using the Langevin dynamics integrator, which introduces a stochastic force to model interactions with the implicit thermal bath at ambient temperature (300 K). The interatomic interactions are computed using `TorchX_MACE_MP_0_L2_2024` potential within the TremoloX framework [15]. The final configuration was extracted from the trajectory and stored for the next analysis.

C. I/V Characteristic

Fig. 2(c) represents the rotaxane-based SMJ we consider for the transport calculations. We calculate the electrical current in the Logic '0' and Logic '1' configurations in QuantumATK v. 2024.09 [12] within the Non-Equilibrium Green's Function (NEGF) framework by using the semi-empirical Slater-Koster Density Functional Tight Binding (SK-DFTB) method for the electronic structure calculation [16], [17]. We calculate the system electrostatics and transport self-consistently, enforcing periodic boundary conditions along x and y directions and Dirichlet boundary conditions along z direction, with conjugate gradient solver for the Poisson equation, and with k-point density of [4,4,150], mesh cutoff at 10 hartree, maximum interaction range 10 Å. The current I is calculated through the Landauer's formula [18]:

$$I_{0,1} = \frac{2q}{h}\int_{-\infty}^{+\infty} TS_{0,1}(E, V_{DS})\,[f_S(E) - f_D(E)]\,dE \tag{2}$$

where q is the electron charge, h is the Planck constant, E is the electron energy, f_S and f_D are source (S) and drain (D) Fermi-Dirac distributions, respectively, and V_{DS} the applied voltage for reading the logic status of the SMJ. TS_0 and TS_1 are the so-called transmission spectra for the configuration Logic '0' and Logic '1', respectively. They correspond to

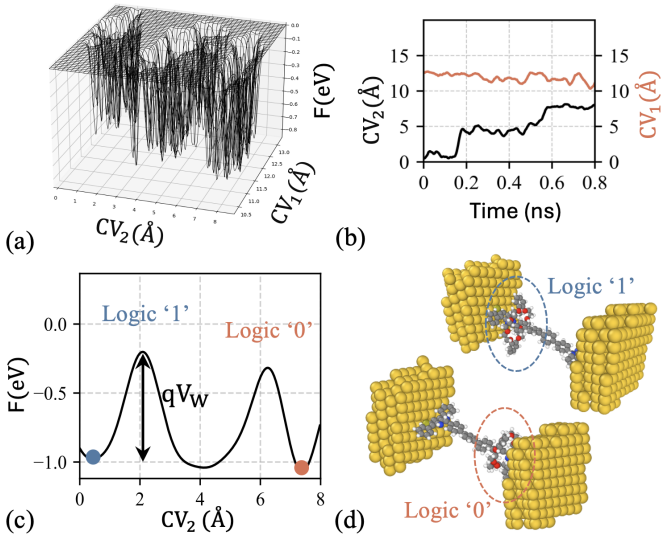

Fig. 3. (a) 3D phase-space of the energy landscape associated to the selected CVs; (b) CV_1 and CV_2 as a function of time for a simulation range; (c) 2D energy landscape associated to the marocycle transition; (d) Molecular conformation derived through ML-FF MD and PEC application.

the S-to-D electron transmission probability, and they depend on the electron energy E and the applied voltage V_{DS}. According to equation 2, because of the Fermi function difference, the relevant portions of $TS_{0,1}$ that contribute to $I_{0,1}$ are those within the Bias Window (BW), i.e. the E range between S and the D Fermi levels, which are displaced of qV_{DS} [19]. The molecular channel energy levels generate TS peaks at specific energies, corresponding to transmission resonances. Whereas, around the system Fermi level E_F, the conduction occurs in off-resonance regime, characterized by S-to-D damped tunneling [4], [18]. To investigate the origin of TS and I differences in the two logic configurations, we make use of the Transmission Pathways (TPs), introduced in [20]. They are a measure of the electron transmission between adjacent atomic sites, and they are graphically represented by arrows, whose dimension is proportional to the magnitude of the transmission, and the verse/color to the direction/phase of the transmission operator.

III. Results and Discussion

A. Barriers Profiling and Logic Configurations

Fig. 3(a) depicts the three-dimensional energy profile as a function of the collective variables (CV_1 and CV_2), offering an overview of the potential energy landscape governing the system dynamics. Stable states, corresponding to local energy minima, are identified, along with two distinct energy barriers that must be overcome for the macrocycle to transition along CV_2. Fig. 3(b) illustrates the evolution of CV_1 and CV_2 during the simulation. The fluctuations observed in these collective variables highlight key transition events corresponding to conformational changes within the molecular system. Analyzing the trends in CV_1 and CV_2 enables the assessment of the intermediate state stability, the presence of metastable configurations, and the efficiency of phase-space exploration achieved during the MetaD simulation. Fig. 3(c) presents a two-dimensional projection of the energy profile, explicitly delineating the transition barriers, both quantified to be approximately 0.8 eV (denoted as qV_W). Moreover, the thermal fluctuations alone are insufficient to drive spontaneous transitions at room temperature, reinforcing the necessity of external excitation mechanisms such as photo-induced or electric field-driven activation. Fig. 3(d) showcases molecular configurations obtained from MD simulations under PEC excitations. These simulations demonstrate how the macrocycle responds to applied external stimuli, facilitating controlled transitions between stable states. The observed structural transformations indicate dynamic switching behavior under appropriate excitation conditions, a crucial feature for molecular-scale memory storage applications. This switching process occurs in two distinct phases: first, the macrocycle undergoes structural rearrangement to prepare for switching, followed by the actual switching event. For the analyzed structure, the switching time is approximately a hundred nanoseconds and can be tuned by recalibrating the structure, for example, by modifying the axle or the macrocycle. In this preliminary approach, the electric field used to facilitate switching and determine the final configurations is an order of magnitude larger than the previously calculated energy barrier.

B. Transport Analysis and State Readout

Fig. 4(a) and Fig. 4(b) report the calculated current-voltage characteristics for the two considered logic configurations in linear and semilogarithmic scales, respectively. I_0 grows linearly with only a limited increase in the trend order above $0.3\,\mathrm{eV}$. Whereas, I_1 exhibits a strongly non-linear behavior. I_1 increases abruptly above $0.4\,\mathrm{eV}$, achieving a peak value of $526\,\mathrm{nA}$ at V_{DS}=$0.455\,\mathrm{eV}$, followed by a sharp Negative Differential Resistance (NDR) region in which I_1 decreases of almost two orders of magnitude. The NDR is a consequence of molecular levels charging [19], which shifts the rotaxane energy levels once they start conducting. This leads to the molecular level exit from the BW, leading to a change of the transport regime from resonance to off-resonance, with a consequent sharp decrease of I_1. For V_{DS}=$0.455\,\mathrm{eV}$ the I_0 is $16.1\,\mathrm{nA}$, i.e., 0.03 times the corresponding I_1. Therefore, a voltage of $0.455\,\mathrm{V}$ can be used to read the logic configuration of the rotaxane-based SMJ, providing well-separated reading currents, being I_1 more than 32 times the corresponding I_0 value.

The different behaviors in the two configurations are clarified by considering TS_0 and TS_1 for $0.455\,\mathrm{V}$ - see Fig. 5(a). The TS_0 behavior within BW is dominated by its peak of 0.023 at $0.18\,\mathrm{eV}$. Similarly, the TS_1 integral in the BW is dominated by its peak of 0.917 at $0.2\,\mathrm{eV}$. Despite the off-resonance contribution around E_F is larger for TS_0 than for TS_1, the different heights of their resonance peaks justify the different I_0 and I_1 values at $0.455\,\mathrm{V}$. Notice that, the resonance vs. off-resonance transmission difference in TS_1 is of about six orders of magnitude, supporting the hypothesis of quantum interference in off-resonance [22]. Moreover, in

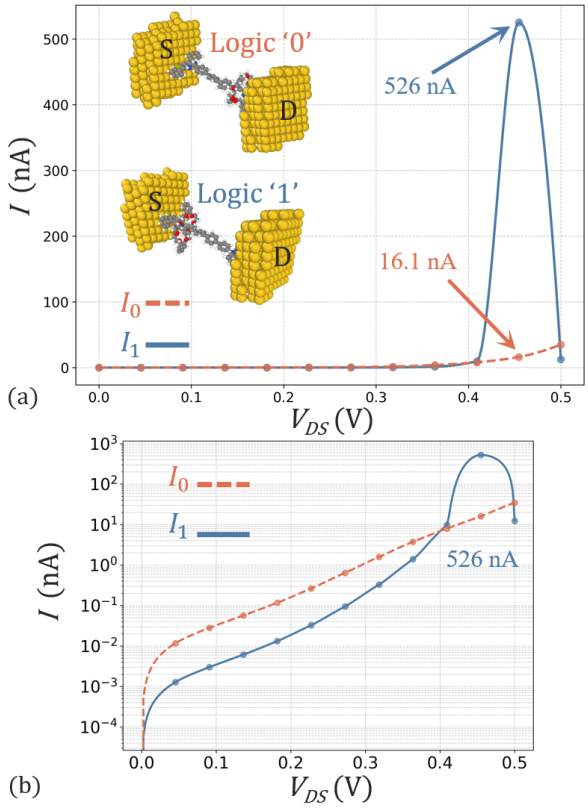

Fig. 4. (a) $I(V)$ characteristics for the logic states '0' (I_0) and '1' (I_1) - the insets show the configurations '0' and '1', respectively; (b) I_0 and I_1 in semilogarithmic scale. The dots are the calculated I-V_{DS} pairs while the lines are their piecewise cubic Hermite polynomial interpolations [21].

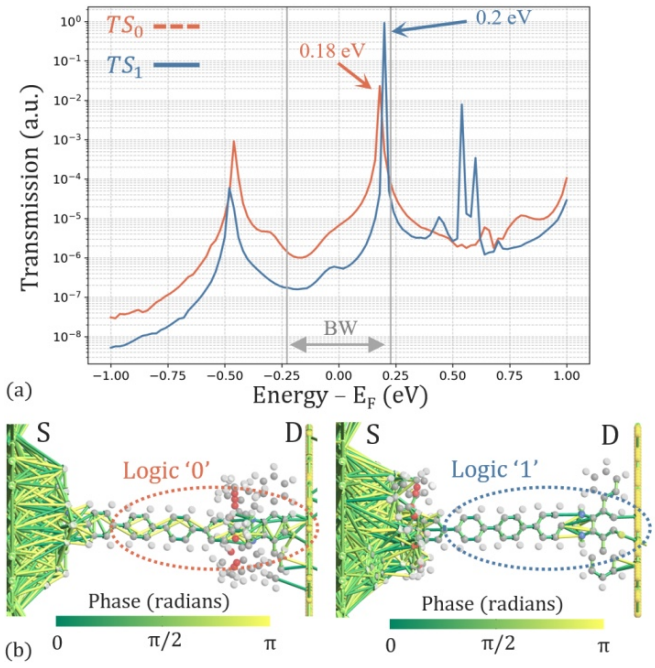

Fig. 5. (a) Piecewise cubic Hermite polynomial interpolated TSs [21] at V_{DS} =0.455 V for the '0' (TS_0) and '1' (TS_1) configurations - the BW is highlighted with vertical grey lines and E_F is the system equilibrium Fermi level; (b) TPs of the configurations '0' (left) at E=0.18 eV, and '1' (right) at E=0.20 eV - the TPs are plotted with the same isovalue.

both cases, the resonance TS peaks are above E_F (0 eV in the graph). Thus they correspond to transmission resonances through the rotaxane's Lowest Unoccupied Molecular Orbital (LUMO). LUMO-dominated conduction is atypical for conjugated systems with thiol anchoring groups [4], [23], [24], thus future works should experimentally validate it or highlight the origin of a simulation artifact.

Finally, to understand the physical origin of the different resonance conditions in the two configurations, we investigate their TPs calculated at the peak E, i.e., E=0.18 eV for the configuration '0' and E=0.2 eV for the configuration '1'. They are reported in Fig. 5(b) left and right, respectively. In the Logic '0' configuration there are relevant electron pathways both from the S to D and from the D to the S. Indeed, visible TPs are going from left (S) to right (D) - green, and from right (D) to left (S) - yellow. Since the latter electron pathways are in phase opposition, they counteract the S-to-D electron transmission and thus they reduce the final value of resonance transmission. In the Logic '1' configuration, instead, there are mainly S-to-D pathways (green) and negligible D-to-S contributions, making the TS_1 resonance peak taller and sharper. The reason behind the TPs difference is in the different rotaxane conformation. In the Logic '0' configuration, the macrocycle is at the D side, supporting the electron tunneling and delocalization at the D side and thus the D-to-channel transmission. In the Logic '1' configuration the macrocycle is instead enhancing the S-to-channel transmission, by adding to the applied voltage.

IV. Conclusions and Future Directions

In this work, we investigated through *ab initio* and semi-empirical simulations the possibility of electrically driving a rotaxane-based SMJ to induce a conformational change and to encode binary information in the macrocycle position within the SMJ. The energy barriers identified at approximately 0.8 eV show that thermal fluctuations alone are insufficient for room-temperature transitions. The MD simulations under PEC excitations demonstrate controllable switching behavior. Furthermore, the two different configurations have relevantly different transmission properties, connected to the different macrocycle position that opposes or enhances the S-to-D transmission features of the SMJ, leading to significantly different electrical currents. At 0.455 V, I_1 is 32 times larger than I_0, enabling the current readout of the logic status of the rotaxane SMJ with safe noise margins. Our results motivate further research efforts in the prototyping and experimental validation of rotaxane-based electrically writable and readable memories, opening the way to highly scaled molecular memories.

V. Acknowledgments

The authors sincerely thank Dr. Luigi Leanza for the introduction to metadynamics, who played a crucial role in achieving the results presented in this article.

REFERENCES

[1] (2023) International roadmap for devices and systems. IEEE. [Online]. Available: https://irds.ieee.org/editions/2023

[2] R. Listo, F. Ravera, G. Beretta, Y. Ardesi, G. Piccinini, and M. Graziano, "Unveiling charge dynamics in molecular field-coupled nanocomputing," in *2024 IEEE 24th International Conference on Nanotechnology (NANO)*, 2024, pp. 424–429.

[3] R. Listo *et al.*, "Unfolding potential and challenges in molecular Field-Coupled nanocomputing," *Nano Futures*, Jan. 2025.

[4] L. Sun, Y. A. Diaz-Fernandez, T. A. Gschneidtner, F. Westerlund, S. Lara-Avila, and K. Moth-Poulsen, "Single-molecule electronics: from chemical design to functional devices," *Chem. Soc. Rev.*, vol. 43, no. 21, pp. 7378–7411, Nov. 2014.

[5] A. Vezzoli, "Mechanoresistive single-molecule junctions," *Nanoscale*, vol. 14, pp. 2874–2884, 2022. [Online]. Available: http://dx.doi.org/10.1039/D1NR06891A

[6] H. M. Osorio *et al.*, "Electrochemical single-molecule transistors with optimized gate coupling," *J. Am. Chem. Soc.*, vol. 137, no. 45, pp. 14 319–14 328, Nov. 2015.

[7] C. E. Spano, F. Mo, Y. Ardesi, M. R. Roch, G. Piccinini, and M. Graziano, "Electronic transport study of bistable cr@ c28 single-molecule device for high-density data storage applications," in *Proceedings of the 8th World Congress on New Technologies (NewTech'22)*, no. 138, 2022, pp. 138–1.

[8] Y. Ardesi, F. Mo, C. E. Spano, G. Ardia, G. Piccinini, and M. Graziano, "Conformation-based molecular memories for nanoscale memcomputing," in *2023 IEEE 23rd International Conference on Nanotechnology (NANO)*, 2023, pp. 694–697.

[9] Y. Ardesi, M. Graziano, and G. Piccinini, "A model for the evaluation of monostable molecule signal energy in molecular field-coupled nanocomputing," *Journal of Low Power Electronics and Applications*, vol. 12, no. 1, p. 13, 2022.

[10] J.-P. Sauvage, "From chemical topology to molecular machines (nobel lecture)," *Angewandte Chemie International Edition*, vol. 56, no. 37, pp. 11 080–11 093, 2017. [Online]. Available: https://onlinelibrary.wiley.com/doi/abs/10.1002/anie.201702992

[11] L. Leanza, C. Perego, L. Pesce, M. Salvalaglio, M. von Delius, and G. M. Pavan, "Into the dynamics of rotaxanes at atomistic resolution," *Chem. Sci.*, vol. 14, pp. 6716–6729, 2023. [Online]. Available: http://dx.doi.org/10.1039/D3SC01593A

[12] S. Smidstrup *et al.*, "Quantumatk: An integrated platform of electronic and atomic-scale modelling tools," *J. Phys: Condens. Matter*, vol. 32, p. 015901, 2020.

[13] G. A. Tribello, M. Bonomi, D. Branduardi, C. Camilloni, and G. Bussi, "Plumed 2: New feathers for an old bird," *Computer Physics Communications*, vol. 185, no. 2, pp. 604–613, 2014. [Online]. Available: https://www.sciencedirect.com/science/article/pii/S0010465513003196

[14] A. Barducci, M. Bonomi, and M. Parrinello, "Metadynamics," *WIREs Computational Molecular Science*, vol. 1, no. 5, pp. 826–843, 2011. [Online]. Available: https://wires.onlinelibrary.wiley.com/doi/abs/10.1002/wcms.31

[15] I. Batatia *et al.*, "A foundation model for atomistic materials chemistry," 2024.

[16] M. Elstner *et al.*, "Self-consistent-charge density-functional tight-binding method for simulations of complex materials properties," *Phys. Rev. B*, vol. 58, pp. 7260–7268, Sep 1998. [Online]. Available: https://link.aps.org/doi/10.1103/PhysRevB.58.7260

[17] K. Stokbro, D. E. Petersen, S. Smidstrup, A. Blom, M. Ipsen, and K. Kaasbjerg, "Semiempirical model for nanoscale device simulations," *Phys. Rev. B*, vol. 82, p. 075420, Aug 2010. [Online]. Available: https://link.aps.org/doi/10.1103/PhysRevB.82.075420

[18] S. Datta, *Quantum Transport: Atom to Transistor*. Cambridge University Press, 2005.

[19] F. Mo, C. E. Spano, Y. Ardesi, M. Ruo Roch, G. Piccinini, and M. Graziano, "Design of pyrrole-based gate-controlled molecular junctions optimized for single-molecule aflatoxin b1 detection," *Sensors*, vol. 23, no. 3, 2023. [Online]. Available: https://www.mdpi.com/1424-8220/23/3/1687

[20] G. C. Solomon, C. Herrmann, T. Hansen, V. Mujica, and M. A. Ratner, "Exploring local currents in molecular junctions," *Nat. Chem.*, vol. 2, no. 3, pp. 223–228, Mar. 2010.

[21] F. N. Fritsch and J. Butland, "A method for constructing local monotone piecewise cubic interpolants," *SIAM Journal on Scientific and Statistical Computing*, vol. 5, no. 2, pp. 300–304, 1984. [Online]. Available: https://doi.org/10.1137/0905021

[22] C. E. Spano, Y. Ardesi, G. Piccinini, and M. Graziano, "Enhancing the on/off current ratio in single-molecule fet via destructive quantum interference," *IEEE Transactions on Electron Devices*, vol. 69, no. 10, pp. 5906–5912, 2022.

[23] G. Wang, T.-W. Kim, and T. Lee, "Electrical transport characteristics through molecular layers," *J. Mater. Chem.*, vol. 21, no. 45, p. 18117, 2011.

[24] L. Cui, R. Miao, C. Jiang, E. Meyhofer, and P. Reddy, "Perspective: Thermal and thermoelectric transport in molecular junctions," *J. Chem. Phys.*, vol. 146, no. 9, p. 092201, Mar. 2017.